B&H Electrical Engineering Volume 14 Special Issue 2020 5-13
sciendo DOI: 10.2478/bhee-2020-0001

Original scientific paper/Izvorni naučni rad

NUMERICAL STUDY OF THERMAL DISSIPATION PROCESSES IN SILICON

NUMERIČKA STUDIJA PROCESA DISIPACIJE TOPLINE U SILICIJUMU

Zlatan Akšamija[1]

Abstract: Heat dissipation in nanoelectronics has become a major bottleneck to further scaling in next-generation integrated circuits. In order to address this problem and develop more energy-efficient nanoelectronic transistor, sensor, and storage devices, we must understand thermal processes at the atomic scale, which requires numerical simulation of the interaction between electrons and heat, carried by quantized lattice vibrations called phonons. Here we examine in detail the phonon emission and absorption spectra in silicon at several elevated values for the electron temperature. The effect of electric field on the electron distribution and equivalent electron temperature is obtained from full-band Monte Carlo simulation for bulk silicon. The electron distributions are used to numerically compute the phonon emission and absorption spectra and discover trends in their behavior at high electron temperatures. The concept of electron temperature is used to understand the relationship between field and heat emission, and it is found that longitudinal acoustic (LA) phonon emission increases at high electron temperatures. It is also found that emission of slower zone-edge phonons increases for all phonon branches at high electron temperatures. These conclusions at high electric fields can be used to enable heat-conscious design of future silicon devices.

Keywords: phonons, thermal properties, Boltzmann transport, scattering rates, CMOS, MOSFET

Sažetak: Prenos toplote u nanoelektronici je postalo glavno usko grlo za dalji razvoj u narednim generacijama visoko integrisanih kola. Da bismo pristupili ovom problemu i razvili efikasnije tranzistore, senzore, i ostale elektronske elemente na nanoskali, moramo proučavati termalne procese na nivou atoma, što zahtijeva numeričku simulaciju interakcije između elektrona i toplote, koju prenose kvantizovane vibracije kristalne rešetke zvane fononi. U ovom radu detaljno ispitujemo spektre emitovanja i absorpcije fonona u silicijumu pri nekoliko povečanih vrijednosti elektronske temperature. Efekat električnog polja na statističku distribuciju elektrona te odgovarajuće temperature elektrona su postignute putem full-band Monte Carlo simulacije rasprostiranja elektrona. Distribucije elektrona se koriste da se numericki izračunaju rate emitovanja i absorpcije fonona te da se sazna o tendencijama njihovih karakteristika pri visokim temperaturama elektrona. Koncept temperature elektrona se koristi da bi se razumio odnos između polja i emitovanje toplote, i došlo se do saznanja da se emitovanje longitudinalnog akustičnog (LA) fonona povečava pri visokim temperaturama elektrona. Također se došlo do zaključka da se prisustvo sporijih fonona sa višim energijama povećava kod svih fononskih polarizacija pri visokim temperaturama elektrona. Ovi zaključci kod visokih električnih polja se mogu koristiti da bi se omogućio razvoj budućih silicijumskih komponenata sa unaprijeđenim termalnim svojstvima.

Ključne riječi: fononi, termalna svojstva, Boltzmannova jednačina, rate rasijavanja, CMOS, MOSFET

INTRODUCTION

Thermal budget is quickly emerging as the prominent limitation on future trends in scaling of semiconductor devices. As new generations of central processing units (CPUs) rely on denser and denser integration of billions of transistors for processing and storage, the transistors themselves are scaled smaller and smaller. This trend is following Moore's Law, coined by Intel's co-founder Gordon Moore, that the number of transistors on a chip doubles every 18 months.

As integrated circuits (ICs) become denser, the heat they dissipate becomes more concentrated and harder to remove, causing the IC to self-heat and limiting its peak operating clock frequency and ultimately its performance. Heat removal is further constrained by the small physical dimensions of ICs and the technological need to further combine them into portable electronics, wearable health monitoring, and other consumer devices where both energy consumption and heat dissipation are undesirable.

To address the issue of heat dissipation, device engineers and circuit designers have long sought to develop more energy-efficient switches and to analyze the impact of selfheating on the performance of individual transistors via device simulation. As device features such as the length of the active channel region inside Complementary Metal-Oxide-Semicondcutor (CMOS) Field Effect Transistors

[1]University of Massachusetts Amherst, 01003 Amherst, MA, U.S.A.
zlatana@umass.edu
Paper submitted: May 2020 Paper accepted: June 2020

(FETs) dip into the single nanometer range, the need for atomistic simulation arises. The widely-used laws governing macroscopic transport of charge and heat begin to falter at scales smaller than the average distance traversed by a carrier between scattering events. The carriers of charge in semiconductors are electrons and holes; their transport at macroscopic scales is described by drift-diffusion equations, which are first-order differential equations that relate local current densities to gradients of the electrostatic potential (voltage) and carrier concentration. Analogously, heat conduction is described by Fourier's law, which gives rise to the widely-used heat equation $\dot{T} = \kappa \nabla^2 T$ with κ being the thermal conductivity, long taken to be a material-specific property. The two equations of current and heat transport can be coupled at the level of total heat dissipation into an electro-thermal description, but this requires prior knowledge of how materials properties vary with temperature.

Both drift-diffusion and the heat equations are continuum representations that fail to capture the particle nature of current, made up of indistinguishable electrons, and heat flux, made up of quantized lattice vibrations called phonons [1]. Being fundamentally local, these continuum laws cannot represent the behavior of electrons and phonons during socalled ballistic (particle-like) motion between randomizing scattering events where they interact. The underlying microscopic picture is that electrons start out in equilibrium undergoing thermal motion; they are accelerated by the electric field coming from the externally applied voltage, whereby they gain energy, followed by scattering of electrons with the lattice vibrations (phonons) when that energy is released as heat via phonon emission. The typical distance an electron travels ballistically between being scattered by a phonon can be only a few nanometers; phonons travel greater distances but at far lowers speeds than electrons (several thousand meters per second compared to the $\approx 10^7$ m/s thermal velocity of electrons), averaging a mean-freepath of about 100-300 nm, depending on temperature and material. At these scales, thermal conductivity becomes nonlocal and strongly a function of device dimensions, geometry, and surfaces [2].

Consequently, at scales of typical transistors in present-day ICs, we must abandon the continuum description of electrothermal transport and turn to an atomistic and statistical description based on the Boltzmann transport equations of electrons and phonons. Further, detailed understanding of electron-phonon coupling, as well as characteristics of the phonon heat generated by the electron current, such as phonon mode and spectrum, are crucial to our understanding of the micro-scale heating issues in semiconductor devices [3]. High electric fields present in ultra-scaled devices pose additional challenges to the understanding of electro-thermal properties as they push the electron population far from equilibrium and can even lead to *hot electrons*, where the proportion of electrons occupying higher energy states far above the edge of the conduction band increases appreciably. Identifying trends in phonon emission spectra at high fields is crucial to enabling more thermally efficient devices. More recently, interest in coupled electro-thermal simulation has grown [4]-[7] due to inherent thermal limitations to electron transport. It is becoming necessary to model accurately the response of phonons to heating due to the release of thermal energy through the electron-phonon interaction. This is significant in the case when electrons are subjected to very high electric fields [8], [9], such as those that are present in the channel region of semiconductor devices.

Previous work in phonon emission in silicon relied on Monte Carlo simulation of electron transport [10]. Such simulations capture the electron-phonon interaction for the purpose of accurately describing the electron current, and usually simplify the treatment of phonons by assuming a simple analytic dispersion relationship between phonon momentum and energy $\hbar\omega(\mathbf{q})$ [8], [11]. This is usually sufficient to describe electron transport with great accuracy. Monte Carlo simulations then keep track of the interactions between electrons and phonons, from which the number of phonons generated during the course of the simulation can be extracted, and the relationship between the net phonon generation rate and the phonon energy can be computed. This was done by Pop et al. [9] for bulk and strained silicon based on analytical isotropic phonon dispersion and analytical multi-valley non-parabolic electron bandstructure. Although the main trends could be identified, lack of full electron bandstructure, and even more importantly the use of analytical isotropic phonon dispersion, did not capture the full detail of the phonon emission spectra. In addition, the Monte Carlo method, due to its stochastic nature, requires a large number of particles and iterations for convergence.

In order to avoid these limitations, we use a deterministic method due to Gilat and Raubenheimer, and extend it to calculate the rate of change of the phonon distribution function due to electron-phonon interactions. In this work, we treat the electron-phonon coupling within the deformation potentials framework, using values given in the literature [11]. We deploy established numerical algorithms for Brillouin zone integration [12] to compute detailed electron-phonon coupling and obtain the rates of phonon emission and absorption by electrons. The electronic band structure is obtained from the empirical pseudo-potential method [13]. In order to capture the band structure more accurately, our implementation was extended to include non-local pseudo-potentials [14], while Weber's adiabatic bond-charge model is used for the phonon dispersion [15]. From our numerical model, we obtain the rates at which phonons are emitted and absorbed by electrons and show that the net emission of phonons scales with the electron temperature, while the spectra of emitted phonons increasingly favor small-wavelength longitudinal phonons. We conclude that heat dissipation in the far-from-equilibrium regime leads to further thermal bottlenecks.

1. NUMERICAL APPROACH

As noted before, phonon transport is described by the Boltzmann transport equation (BTE), which describes the evolution in time of the phonon distribution function. This distribution function, denoted by $N(\mathbf{r},\mathbf{q},t)$, represents the average number of phonons which occupy a state $\mathbf{q}$ in position $\mathbf{r}$ and at time t. The rate of change of the phonon distribution has several contributions. One of the dominant contributions is due to the anharmonic phonon processes, which arise due to third and higher order components of the bond forces. This is a phonon-phonon interaction which allows the phonon population to return to equilibrium when perturbed by a temperature gradient or a generation source [16]. A second contribution which is strongly present in semiconductor devices is due to the generation of phonons by the electron-phonon interaction. This interaction occurs when strong electric fields drive the electron population out of equilibrium and impart energy on the electrons. The electronphonon interaction is the primary means for electrons to release the energy accumulated from the accelerating effect of the applied electric field and to return to equilibrium. This is especially important in nanoscale transistor devices, where electrons are accelerated by the strong fields in the channel region of the transistor, and then the electrons have to release energy in the form of phonons in order to return to quasiequilibrium in the drain region before they leave the transistor through the contacts.

Generation as well as absorption of phonons couple together the electron and phonon populations and allow energy exchange between them, leading to a net flow of energy from the electron gas to the phonon bath. The phonon population under the heating effect of electrons can be described by the phonon BTE with the added term due to the electronphonon interaction [17]. The phonon distribution function, notated by $N(\mathbf{r},\mathbf{q},t)$, increases every time an electron-phonon scattering event takes place, and decreases for every anharmonic phonon decay. Therefore we will have two terms on the right-hand-side, one owing to the interactions of phonons with electrons, and the other due to interactions of phonons with other phonons through anharmonic decay, boundary scattering, isotope scattering, and other interaction mechanisms which are beyond the scope of this work:

$$\frac{\partial N(\mathbf{r},\mathbf{q},t)}{\partial t}+\mathbf{v}(\mathbf{q})\nabla_{\mathbf{r}}N(\mathbf{r},\mathbf{q},t)=\left(\frac{dN(\mathbf{r},\mathbf{q},t)}{dt}\right)_{el-ph}-\left(\frac{dN(\mathbf{r},\mathbf{q},t)}{dt}\right)_{ph-ph} \quad (1)$$

In considering this challenging seven-dimensional transport equation, having, in general, 3 dimensions for position, 3 for crystal momentum, often called *reciprocal space*, and 1 for time, we will restrict our attention to homogenous materials in the steady state and drop the position variable $\mathbf{r}$. In steady-state, all variation with time has vanished, so that the first term containing a partial derivative with respect to time can be removed. The homogenous restriction means we are considering the case of bulk material, so that all gradients with respect to the spatial coordinate are zero. This removes from consideration the second term of the phonon Boltzmann Transport equation containing spatial gradients of the phonon distribution function. Finally, the term due to anharmonic decay is usually treated in the relaxation time approximation, and the relaxation rates have been presented by several researchers [18], [19] based on analytical models of the phonon dispersion, as well as detailed numerical computations of decay rates of optical phonons based on an empirical model of phonon dispersion [20] and Density Functional Theory (DFT) [21]. On the other hand, the generation term due to electron-phonon interaction has not been given the same amount of attention, as it does not play a significant role in purely thermal transport, and contributes little when there are no electric fields present because the electron population is in equilibrium with phonons.

The rate of change of the phonon distribution function due to electron-phonon scattering can can be computed by combining the contributions from the electron-phonon scattering over all electron momenta. We notice that for every transition an electron makes between an initial state $\mathbf{k}$ to a final state $\mathbf{k'}$, a phonon with a momentum $\mathbf{q} = \pm(\mathbf{k}-\mathbf{k'})$ is either absorbed or emitted, depending on the energies of the two electron states. Every emission increases the phonon occupancy and adds one to $N(\mathbf{k})$, while every phonon absorption does the opposite, and decreases $N(\mathbf{q})$ by unity [22]. The electron states are weighted by their probability of occupancy, given by the electron distribution function $f_e(k)$. The total rate of change of the phonon distribution function is obtained by summing over all the electron states [23], as shown in (2):

$$\left(\frac{dN(\mathbf{q})}{dt}\right)_{el-ph}=\sum_{\mathbf{k}}\frac{|D(\mathbf{q})|^2 I^2(q)}{\rho\omega(\mathbf{q})}\left(N(\mathbf{q})+\frac{1}{2}\pm\frac{1}{2}\right) f_e(\mathbf{k})\delta\left(E(\mathbf{k})-E(\mathbf{k}\pm\mathbf{q})\pm\hbar\omega(\mathbf{q})\right) \quad (2)$$

In this work, we are interested in bulk silicon crystal, which is taken to be infinite in extent. This implies that momentum states are also infinite in number, so they form a countable continuum. In this limit, the summation over all momentum states $\mathbf{q}$ has been shown to approach an integral over the entire first Brillouin zone for the purpose of calculation [24]:

$$\left(\frac{dN(\mathbf{q})}{dt}\right)_{el-ph}=\frac{2\pi}{\Omega}\iiint d\mathbf{k}\frac{|D(\mathbf{q})|^2 I^2(q)}{\rho\omega(\mathbf{q})}\left(N(\mathbf{q})+\frac{1}{2}\pm\frac{1}{2}\right) f_e(\mathbf{k})\delta\left(E(\mathbf{k})-E(\mathbf{k}\pm\mathbf{q})\pm\hbar\omega(\mathbf{q})\right) \quad (3)$$

Energy conservation is expressed by the δ-function, which defines a complex energy-conserving surface in the first Brilluoin zone. Using properties of the δ-function, the integral over $\mathbf{k}$ is converted into a surface integral over the entire energy-conserving surface (4):

$$\left(\frac{dN(\mathbf{q})}{dt}\right)_{el-ph} = \frac{2\pi}{\Omega} \oiint_{E(\mathbf{k})-E(\mathbf{k}\pm\mathbf{q})=\pm\hbar\omega(\mathbf{q})} \frac{d\mathbf{S}}{\left|\nabla_{\mathbf{k}} E(\mathbf{k}) - \nabla_{\mathbf{k}} E(\mathbf{k}\pm\mathbf{q})\right|}$$
$$\frac{\left|D(\mathbf{q})\right|^2 I^2(q)}{\rho\omega(\mathbf{q})}\left(N(\mathbf{q})+\frac{1}{2}\pm\frac{1}{2}\right) f_e(\mathbf{k}) \qquad (4)$$

where the closed surface of integration is defined by energy conservation to include all points $\mathbf{k}$ such that the equality $E(\mathbf{k}) - E(\mathbf{k}) = \pm\mathbf{q}$ is satisified. At the same time, this surface contains contributions from all the final momentum states k' which are also able to conserve crystal momentum with a given inital state k. The contribution to the integral from each small cube in momentum space is given by the area of the intersection between this energy-conserving surface and that particular cube, weighted in our case by the contribution from the matrix element. Such an integral over the entire first Brillouin zone can be computed numerically by dividing the Brillouin zone into a regular mesh of small cubes or tetrahedra, and computing the area of intersection of the energy isosurface with each particular cube or tetrahedron. There are several algorithms that are well-suited for the purpose of such a calculation. We choose the algorithm due to Gilat and Raubenheimer, which uses a division of the crystal momentum into regular small cubes, then expanding all the terms in the integrand to first order for the purpose of obtaning a very accurate result and taking into account the strong gradients in electron energy and distribution functions. Due to the inclusion of up to linear terms, this approach was also termed *Linear Analytic* [12]. This algorithm was first proposed for the purpose of calculating spectral properties, such as the density of states. The Gilat-Raubenheimer (GR) approach has also been applied to a very accurate calculation of the electron-phonon scattering rates in silicon and other semiconductors by Fischetti and Laux [11].

$$\left(\frac{dN(\mathbf{q})}{dt}\right)_{el-ph} = \frac{\left|D(\mathbf{q})\right|^2 I^2(q)}{\rho\omega(\mathbf{q})}\left(N(\mathbf{q})+\frac{1}{2}\pm\frac{1}{2}\right)\sum_i S_i(\mathbf{k}_i) f_e(\mathbf{k}_i)$$

In the GR algorithm, the portion of the energy-conserving surface in each small discretization cube is assumed to be a plane so that every point on the plane is perpendicular to the gradient at the center of the cube. The shape of the intersection of a plane and a cube then becomes either a triangle, quadrangle, or pentangle, depending on the angle of the gradients of the electron energy bandstructure in each particular cube, which are precomputed on the same mesh as the energies, as described earlier. The contribution S_i arising from each small cube centered at $\mathbf{k}_i$ and indexed by i in the entire Brillouin zone can then be computed based on geometric considerations, and summed together to obtain the total rate of change of the phonon distribution function $N(\mathbf{q})$, as given in (5). Further details of the Gilat-Raubenheimer *Linear Analytic* algorithm, and the expressions for the areas of intersections of equal energy surfaces with cubes in momentum space are given in [25]. This algorithm is very accurate since it uses extrapolation and well-suited to using tabulated data for bandstructures and dispersions [12]. Unlike the work of Fischetti and Laux, who used an analytical expression for the dispersion relationship of phonons, we use the full dispersion computed from Weber's Adiabatic Bond Charge model in order to accurately obtain the dependance on momentum of the phonon energy $\hbar\omega(\mathbf{q})$ in the integrand of equation (3). This model allows a very accurate representation of all phonon branches, shown in Figure 1, even along directions other than the main symmetry directions [26].

The deformation potential for acoustic phonon interaction, due to the crystal symmetry, reduces to two independent parameters: the dilatation potential Ξ_d and the uniaxial shear

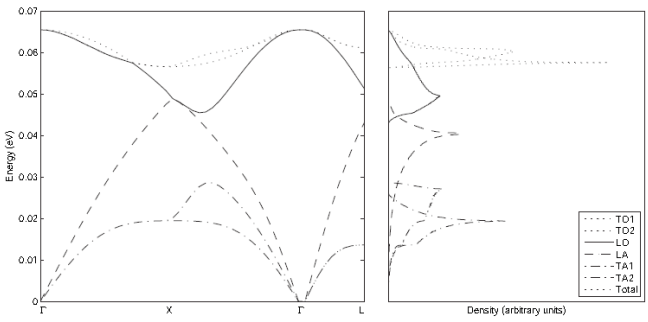

Figure 1: Phonon dispersion relationship (left) and phonon density-of-states (DOS) for each of the 6 phonon branches and total (right). The Adiabatic Bond Charge model is used to compute the phonon frequencies on a regular grid in momentum space, thereby allowing the DOS to be computed by the method of Gilat and Raubenheimer. The phonon DOS is found to be dominated by optical and longitudinal acoustic (LA) modes due to their flat dispersion curves and low group velocities, especially near the Brillouin zone edge. The DOS also shows that the optical modes are found above 48meV, transverse acoustic (TA) modes are below 25meV, and LA modes are between.

potential Ξ_d [27], [22]. The relationship between the deformation potential and these two parameters is described by the Herring-Vogt relation, which expresses the acoustic deformation potential in terms of the dilatation and shear potentials, along with an angular dependence. The angular dependence is on Θ, the angle between the phonon momentum $\mathbf{q}$ and the longitudinal axis of the conduction-band valley [28]. The acoustic deformation potential also depends on the phonon polarization, which can be either longitudinal or transverse, and is expressed in (5):

$$D_{LA(q)} = \left(\Xi_d + \Xi_u cos^2\Theta\right) q$$
$$D_{TA(q)} = \left(\Xi_u sin\Theta cos\Theta\right) q \qquad (5)$$

For optical phonons, the interaction is of the zero-th order and the deformation potential, expressed in (6), is taken to be a constant with values taken from [11]. The overlap integral between the cell portions of the Bloch states [28] is computed in the Nordheim, sometimes called the spher-

ical cell, approximation [29]. This provides an analytical expression for the integral (7), which depends only on the magnitude of momentum of the phonon being exchanged $\mathbf{q} = |\mathbf{k} - \mathbf{k}'|$. The $R_s = a_{Si}[3/(16\pi)]^{1/3}$ is the radius of the Wigner-Seitz cell.

$$D_{LO,TO(q)} = DK_{op} \tag{6}$$

$$I(q) = \frac{3}{(qR_s)^3}\left[sin(qR_s) - qR_s cos(qR_s)\right] \tag{7}$$

The electron and phonon populations are assumed to be initially in equilibrium, with a Fermi distribution (8) for electrons, and a Bose-Einstein distribution (9) for phonons [30]. The electric field is introduced through a fullband Monte Carlo ensemble electron simulation, described in earlier work [31], [32]. The term *full-band* here means that the simulation uses a numerically computed electronic structure to accurately describe electronic states an the relationship between their crystal momentum, velocity, and energy without resorting to approximations such as effective mass. The simulation tracks an ensemble of electrons, typically 100000 in size, as they are accelerated by the electric field and undergo a sequence of electron-phonon scattering events until it converges to a non-equilibrium electron distribution which includes the effect of the applied electric field. This provides us with an accurate distribution for electrons [33]. The effect of the applied electric field can then be understood through the concept of equivalent electron temperature T_e [24], which captures the heating of the electron population from the energy imparted on them by the electric field. Increasing the applied field imparts more energy on the electron population and pushes the electron temperature further up above the lattice (phonon) temperature T_{ph}. The imbalance means electrons and phonons are out of equilibrium and results in a net transfer of energy from electrons to phonons. This transfer is our microscopic description of heat dissipation.

Fitting the semi-logarithmic plot of the Monte Carlo results for the electron distributions at various applied electric fields, as shown in Figure 2, allows us to extract the electron temperature from each distribution and relate it to the applied electric field. In order to account for the effect of electric field on the electron, and ultimately the phonon population, we use a quasi-equilibrium distribution for electrons based on the Fermi-Dirac distribution with the appropriate electron temperature determined from the fit to Monte Carlo results at each given electric field.

$$f(\mathbf{k}) = \left[exp\left(\frac{E(\mathbf{k}) - E_F}{k_B T_e}\right)\right]^{-1} \tag{8}$$

$$N(\mathbf{q}) = \left[exp\left(\frac{\hbar\omega(\mathbf{q})}{k_B T_{ph}}\right) - 1\right]^{-1} \tag{9}$$

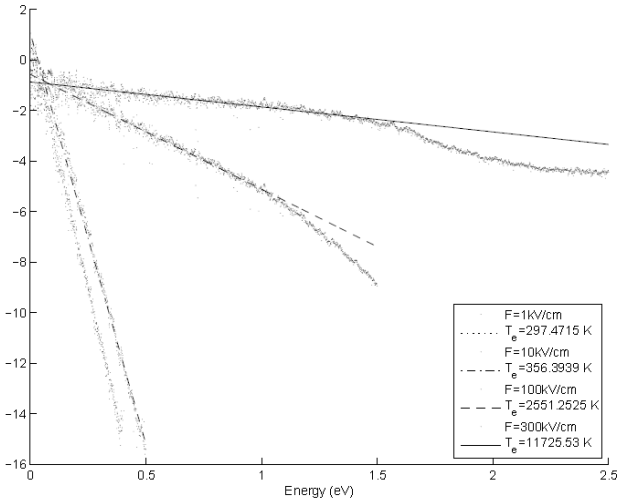

Figure 2: Logarithmic plot of the electron distribution histogram. This figure demonstrates that the electron distributions remain linear over the range of energies of interest, even at high applied electric fields. This allows the definition of an equivalent electron temperature T_e which reflects the heating of the electron population by the applied electric field.

The gradient of the electron energy can be large and the numerical accuracy of the Brillouin zone algorithm in [25] can be improved by expanding the electron distribution function up to first order and including the linear terms, as given in [34]. The gradient of the quasi-equilibrium electron distribution function, (8), can be determined analytically as in (10), while the gradients of the electron energies can be computed numerically and tabulated along with the results for the electron energies. This improvement means we can incorporate the gradient into the summation in (5) in order to obtain a more accurate method, thereby improving the quality of final results for phonon emission and absorption rates calculated from the electron distributions.

$$\begin{aligned}\nabla_{\mathbf{k}} f(\mathbf{k}) &= \frac{\partial f(E)}{\partial E}\nabla E(\mathbf{k}) \\ &= -\frac{1}{k_B T} f(\mathbf{k})\left(1 - f(\mathbf{k})\right)\nabla E(\mathbf{k})\end{aligned} \tag{10}$$

Because the integral in (5) is over all electron states $\mathbf{k}$, terms depending only on the phonon momentum $\mathbf{q}$ have been removed from the integral. In addition, due to its dependence on the phonon momentum $\mathbf{q}$ only, the phonon distribution function $N(\mathbf{q})$ can be factored out of the integral in (5) and divided by it to obtain a rate $\Gamma(\mathbf{q}) = 1/N(\mathbf{q})\,(dN(\mathbf{q})/dt)$. The dependence of this rate on the phonon energy ω, rather than momentum $\mathbf{q}$, is obtained by averaging over all modes ear a given energy ω using the same Gilat-Raubenheimer approach (11). The phonon emission spectrum Γ is then scaled by the phonon density-of-states (DOS), shown in Figure 1:

$$\Gamma(\omega) = \frac{\int \Gamma(\mathbf{q})\partial\left(\omega - \omega(\mathbf{q})\right)d\mathbf{q}}{\int \partial\left(\omega - \omega(\mathbf{q})\right)d\mathbf{q}} \tag{11}$$

This converts the distribution from momentum space into an energy spectrum $\Gamma(\omega)$, and enables us to examine the results. Each of the phonon types can be identified with a

particular energy range. The DOS in Figure 1 shows that the optical modes are found above 48 meV, transverse acoustic (TA) modes are below 25 meV, and LA modes are in between. We can therefore examine trends in these three phonon types by looking at their respective energy ranges, low for TA, high for optical, and middle for LA phonons.

2. RESULTS AND DISCUSSION

Due to the large differences in the directions and velocities of phonon propagation for different phonon modes, examining how much of each phonon polarization is generated is important for understanding heating in silicon at the nanoscale. Transverse optical modes (TO) have very flat dispersion curves, and consequently have the lowest velocities, as shown in Figure 3. The longitudinal optical mode (LO) also tends to zero in the long-wavelength limit, but its velocity increases for short wavelength phonons.

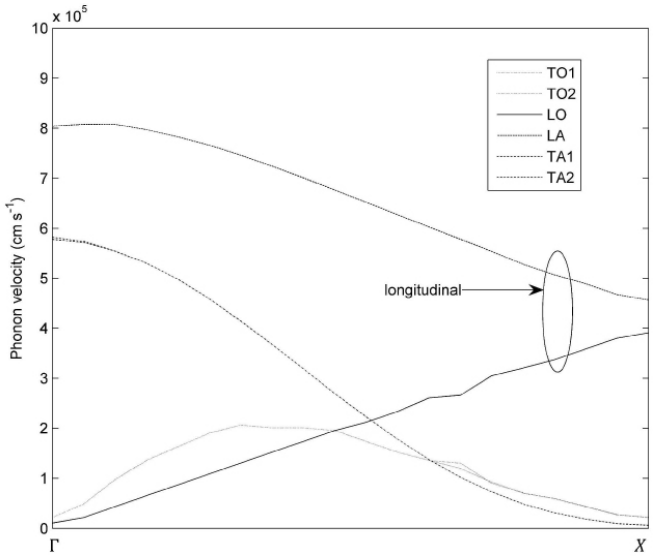

Figure 3: Plot of phonon velocities. Group velocity is given by the gradient of the phonon dispersion relation. Phonon velocities dictate how fast each mode can propagate heat through the silicon lattice. Longitudinal modes (dashed line), especially the longitudinal acoustic mode, have the highest velocity. Transverse acoustic (TA) modes are slower, while the optical modes are very slow due to their flat dispersion.

The transverse acoustic (TA) modes have larger velocities, and approach the speed of sound in the long-wavelength limit. The highest velocities are present for the longitudinal acoustic mode (LA) due to the fact that longitudinal waves propagate along the directions of the bonds in the crystal lattice. Phonon velocities can be averaged over all modes near a particular energy to obtain a velocity spectrum $v(\omega)$ which depends on phonon energy ω rather than the three-dimensional momentum vector $\mathbf{q}$, and is therefore more suitable for plotting and comparisons. This is done by integrating phonon velocities over the energy isosurface, and then scaling by the density-of-states, as in (12). The velocity spectrum $v(\omega)$, shown in Figure 4, demonstrates that phonon velocities for each mode are highest at low energy, for phonons near the Brillouin zone center, and lower for higher energy zone-edge phonons.

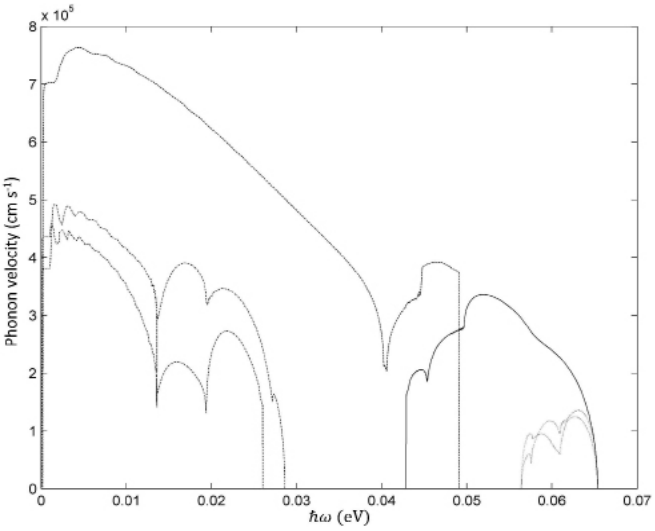

Figure 4: Plot of phonon velocity spectra. For each energy value on the xaxis, the velocity is computed by numerically averaging over the energy isosurface. This plot shows the average phonon velocity at each particular energy rather than momentum or direction. Longitudinal acoustic mode (dashed line) has the highest velocity. Transverse acoustic (dash-dot) and the optical modes (dotted line) are slower due to their flat dispersion, especially at higher energies corresponding to phonons near the Brillouin zone boundary.

$$v(\omega)=\frac{\int \nabla\omega(\mathbf{q})\partial\big(\omega-\omega(\mathbf{q})\big)d\mathbf{q}}{\hbar\int \partial\big(\omega-\omega(\mathbf{q})\big)d\mathbf{q}} \tag{12}$$

In Figure 5 and 6, we find that phonon absorption is strongly dominated by transverse acoustic (TA) phonons. Curves are presented for electron temperatures ranging from 300 K (bottom curve) up to 10000 K (top curve), corresponding to electric fields from 1 kV/cm up to around 300 kV/cm.

Both emission and absorption are in units of inverse seconds. Increasing the applied electric field has the effect of increasing the difference between the electron temperature T_e and the lattice temperature T_{ph}. This difference acts to increase both the emission and absorption spectra, and favors higher energy acoustic phonons. There is an overall flattening of the emission spectrum, where the largest increases can be noted in zone-edge (short wavelength) acoustic (TA and LA) modes, while, to a lesser extent, the trend reverses for optical modes. The trend is especially pronounced for modes near the Brillouin zone edge, at energies around 48 meV for LA phonons, and 55 meV for optical phonons. TA phonon emission is strongest at low electron temperatures, where both emission and absorption are dominated by small-energy (long-wavelength) phonons, while the opposite is true at high electron temperatures, where the largest increase is also in the zone-edge phonons, at energies around 25 meV. LA phonons have the highest propagation velocities of all phonon polarizations, Figure 3, so they are expected to carry the emitted thermal energy fastest. Further, optical phonons which have very short lifetimes, and quickly

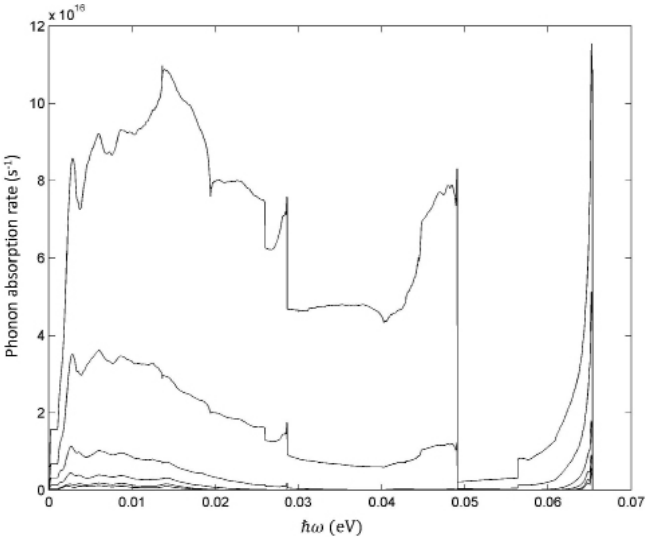

Figure 5: Plot of the rate of phonon absorption (per second) for electron temperatures ranging from 300 K (bottom curve) up to 10000 K (top curve), corresponding to electric fields from 1 kV/cm up to around 300 kV/cm. Increase in the applied field causes a difference between T_e and lattice temperature T_{ph} and acts to increase the rate of absorption, especially in the LA and optical modes.

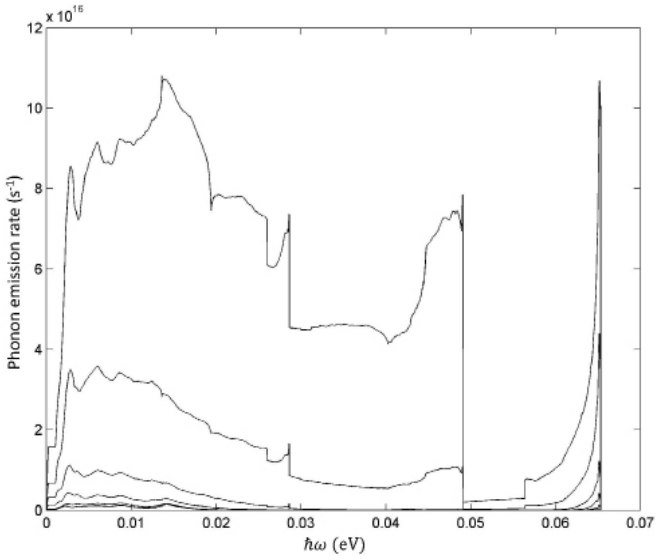

Figure 6: Plot of the rate of phonon emission (per second) for electron temperatures ranging from 300 K (bottom curve) up to 10000 K (top curve),corresponding to electric fields from 1 kV/cm up to around 300 kV/cm. Rate of phonon absorption increases with the temperature of electron distribution, and favors higher energy and zone-boundary phonons. At the highest electron temperature of 10000 K, we can see sharp increases in the emission of phonons near the highest energy for each mode. This is most prominent in LA phonons, around 48 meV, and TA modes near 25 meV.

decay into combinations of acoustic phonons, while LA phonons have longer mean-freepaths of around 100 nm [5] and longer lifetimes; even after anharmonic decay, they do not necessarily fully equilibrate [35].

As shown in Figure 4, small energy TA phonons are faster than their zone-edge counterparts, so we can expect an increasing proportion of the heat to be carried by LA phonons at high electron temperatures, corresponding to high electric fields. Similar conclusions can be drawn from the logarithmic plot of the net phonon generation rate, shown in Figure 7. The logarithmic plot shows a nearly linear dependence of the optical phonon generation on phonon energy, indicating an exponential relationship between phonon frequency and generation rate. The most drastic dependence on the electric field strength and electron temperature is again in the LA phonon branch, which increases from very small contributions at low fields to nearly even levels with the optical phonon generation at very high electric field strengths. This is especially true for higher energy LA and LO phonons with energies near 48 meV corresponding to short wavelength phonons near the Brilloin zone edge. These results and trends agree with Monte Carlo calculations of emission spectra in silicon [9] and similar results for a silicon device [5]. Both of the prior Monte Carlo calculations showed that the largest increase in the phonon emission at high electric fields is in the LA modes around 40 meV, in qualitative agreement with our results. More recently, Fischetti et al. [35] showed that the total energy loss from electrons is strongest to the TA phonon branch, followed by the optical (TA and TO) branches, with LA phonons taking up the least dissipation; while we did not evaluate the total energy by phonon branch, our results do support the view that acoustic phonons dominate the net emission spectra.

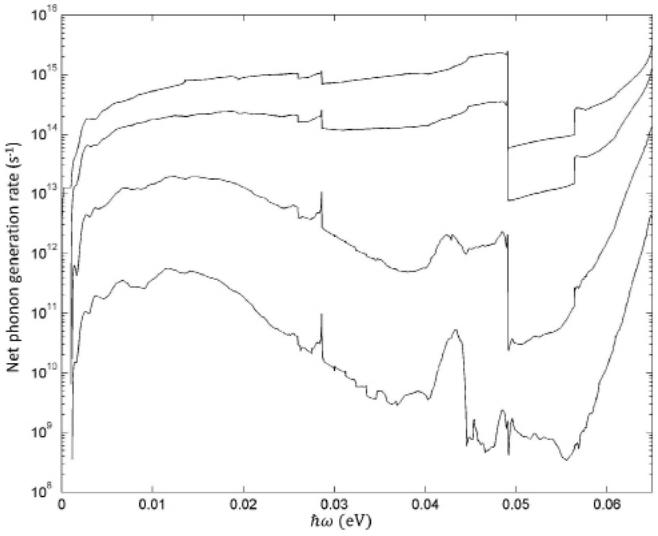

Figure 7: Logarithmic plot of the net rate of phonon generation (per second) for electron temperatures ranging from 300 K (bottom curve) up to 10,000 K (top curve), corresponding to electric fields from 1 kV/cm up to around 300 kV/cm. This rate is computed from the difference between the total emission and absorption rates, and represents the net increase of the phonon distribution function due to coupling between electrons and phonons. The logarithmic plot is linear in the optical region indicating an exponential energy dependence of emission in the optical branches. This plot also shows that the most dramatic increase with increasing electic field and electron equivalent temperature is in the longitudinal acoustic branch, especially near the end of the Brillouin zone at energies around 48 meV.

Lastly, we examine the relationship between emission and absorption spectra. Figure 8 shows that the ratio of emission and absorption follows a Boltzmann factor $exp(\hbar\omega/k_B T_e)$ at the electron temperature T_e, rather than the lattice, or phonon, temperature. This ratio is smaller for high electron temperatures, and for optical phonons. When electron and phonon temperatures are equal, we have equilibrium, and detailed balance holds, producing a ratio equal to the Boltzmann factor. When the electron and phonon populations are out of equilibrium, the electron temperature is higher, producing a net excess of emission over absorption so that the net heat dissipation is ultimately proportional to the difference between electron and phonon temperatures. Nonetheless, the shape of the spectrum of the emitted phonons is not static; rather, it evolves with the electron temperature and depends on the difference between the electron and the lattice temperatures.

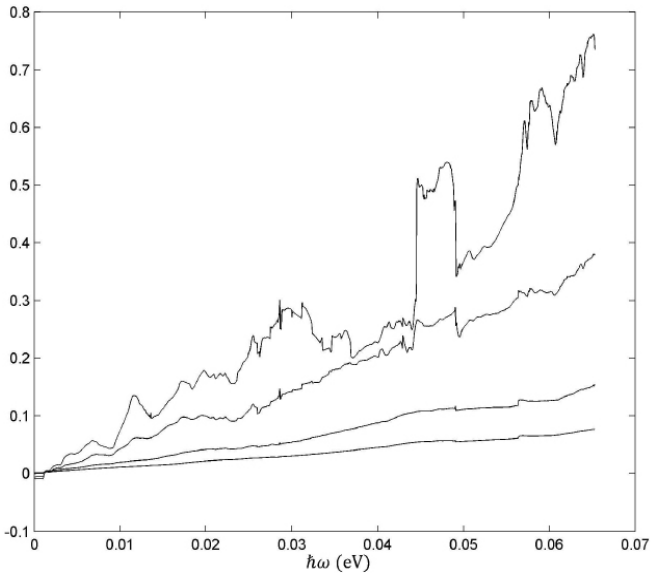

Figure 8: Plot of the logarithm of the ratio of phonon emission to absorption for electon temperatures ranging from 1000 K (top curve) up to 10000 K (bottom curve), corresponding to electric fields from 50 kV/cm up to around 300 kV/cm. The slope of each curve corresponds to the electron temperature of the distribution from which it was calculated, indicating that the ratio of emission and absorption is given by a Boltzmann factor at the electron temperature T_e.

3. CONCLUSION

We examined the nature of phonon generation in silicon at several strengths of applied electric field. We identified several trends, in particular that phonon emission at low and intermediate fields is dominated by low-energy transverse acoustic phonons. As the temperature of the electron population increases under the acceleration of the applied electric field, the rate of net emission of longitudinal acoustic and optical phonons approaches that of TA modes. Overall, high electron temperatures push the phonon spectra towards higher energies. This favors LA modes the most, and may shift the subsequent transport of heat more from TA to LA modes. Due to longer lifetimes, lower velocity, and focused propagation of LA modes, design optimizations may be possible and necessary in future devices. These may include changing the orientation of the active channel region of a nanowire MOSFET device to coincide with the propagation directions of the LA phonons to avoid trapping phonons inside the critical active region of MOS transistors.

REFERENCES

[1] Z. Aksamija. U. Ravaioli: Joule heating and phonon transport in silicon MOSFETs, Journal of Comput. Electron., vol. 5, no. 4, pp. 431-434, 2006

[2] Z. Aksamija, I. Knezevic: Anisotropy and boundary scattering in the lattice thermal conductivity of silicon nanomembranes, Phys. Rev. B, 82.045319, July 2010

[3] S. Sinha, K. E. Goodson: Phonon heat conduction from nanoscale hotspots in semiconductors. In Heat Transfer 2002, Proceedings of the Twelfth International Heat Transfer Conference, pp. 573–578, 2002

[4] J. Lai, A. Majumdar: Concurrent thermal and electrical modeling of sub-micrometer silicon devices, Journal of Applied Physics, vol. 79, no. 9, pp. 7353-7361, 1996

[5] J.A. Rowlette, K.E. Goodson: Fully coupled nonequilibrium electronphonon transport in nanometer-scale silicon fets, Electron Devices, IEEE Transactions on, vol. 55, no. 1, pp. 220-232, Jan. 2008

[6] M. Mohamed, Z. Aksamija, W. Vitale, F. Hassan, K.-H. Park, U. Ravaioli: A conjoined electron and thermal transport study of thermal degradation induced during normal operation of multigate transistors, IEEE Trans. Electron Devices, vol. 66, pp. 976-983, 2014

[7] M. Mohamed, K. Raleva, U. Ravaioli, D. Vasileska, Z. Aksamija: Phonon dissipation in nanostructured semiconductor devices: Dispersing heat is critical for continued integrated circuit progress, IEEE Nanotechnology Magazine, vol. 13, no. 4, pp. 6-17, 2019

[8] E. Pop, R. W. Dutton, K. E. Goodson: Analytic band Monte Carlo model for electron transport in Si including acoustic and optical phonon dispersion, Journal of Applied Physics, vol. 96, no. 9, pp. 4998–5005, November 2004

[9] E. Pop, R. W. Dutton, K. E. Goodson: Monte Carlo simulation of Joule heating in bulk and strained silicon, Applied Physics Letters, vol. 86, pp. 082101–082103, 2005

[10] Z. Aksamija, U. Ravaioli: Energy conservation in collision broadening over a sequence of scattering events in semiclassical monte carlo simulation, Journal of Appl. Phys., vol. 105, 083722, April 2009

[11] M. V. Fischetti, S. E. Laux: Monte Carlo analysis of electron transport in small semiconductor devices including band-structure and space-charge effects. Physical Review B, vol. 38, no. 14, pp. 9721–9745, November 1988

[12] G. Gilat: Analysis of methods for calculating spectral properties in solids, Journal of Comp. Phys., vol. 10, no. 3, pp. 432–465, Dec. 1972

[13] Marvin L. Cohen, T. K. Bergstresser: Band structures and pseudopotential form factors for fourteen semiconductors of the diamond and zinc-blende structures, Phys. Rev., vol. 141, no. 2, pp. 789–796, Jan 1966

[14] J. R. Chelikowsky, Marvin L. Cohen: Nonlocal pseudopotential calculations for the electronic structure of eleven diamond and zinc-blende semiconductors, Phys. Rev. B, vol. 14, no. 2, pp. 556–582, Jul 1976
[15] O. H. Nielsen, W. Weber: Lattice dynamics of group IV semiconductors using an adiabatic bond charge model, Computer Physics Communications, vol. 18, pp. 101–107, 1979
[16] Z. Aksamija, U. Ravaioli: Anharmonic decay of g-process longitudinal optical phonons in silicon, Appl. Phys. Lett., vol. 96, no. 9, pp. 091911-1 - 091911-3, 2010
[17] S. Sinha, E. Pop, R. W. Dutton, K. E. Goodson: Non-equilibrium phonon distributions in sub-100 nm silicon transistors, Journal of Heat Transfer, vol. 128, pp. 638–647, 2006
[18] M. G. Holland: Analysis of lattice thermal conductivity, Phys. Rev., vol. 132, no. 6, pp. 2461–2471, Dec 1963
[19] J. Callaway: Model for lattice thermal conductivity at low temperatures. Phys. Rev., vol. 113, no. 4, pp. 1046–1051, Feb 1959
[20] B. P. Allen: A tetrahedron method for doubly constrained brillouin zone integrals application to silicon optic phonon decay, Phys. Stat. Sol. B, vol. 120, no. 2, pp. 529–538, 1983
[21] A. Debernardi, S. Baroni, E. Molinari: Anharmonic phonon lifetimes in semiconductors from density-functional perturbation theory, Phys. Rev. Lett., vol. 75, no. 9, pp. 1819–1822, Aug 1995
[22] E. M. Conwell: High Field Transport in Semiconductors, Academic Press, Inc., New York, 1967
[23] B. K. Ridley: Quantum Processes in Semiconductors, Clarendon Press, Oxford, 1998
[24] K. Hess: Advanced Theory of Semiconductor Devices, IEEE Press, New York, 2000
[25] G. Gilat, L. J. Raubenheimer: Accurate numerical method for calculating frequency-distribution functions in solids, Phys. Rev., vol. 144. no. 2, pp.390–395, Apr 1966
[26] W. Weber. Adiabatic bond charge model for the phonons in diamond, Si, Ge, and U-Sn, Physics Reviews B, vol. 15, pp. 4789–4803, May 1977
[27] G. L. Bir, G. E. Pikus: Symmetry and Strain-Induced Effects in Semiconductors, Halsted Press, New York, 1974
[28] D. K. Ferry: Semiconductor Transport, Taylor and Francis, New York, 2000
[29] T. A. Bak: Phonons and Phonon interactions, W. A. Benjamin, Inc., New York, 1964
[30] C. Kittel: Introduction to Solid State Physics, John Wiley and Sons, Inc., New York, 2005
[31] A. Duncan, U. Ravaioli, J. Jakumeit: Full-band monte carlo investigation of hot carrier trends in the scaling of metal-oxidesemiconductor field-effect transistors, IEEE Transactions on Electron Devices, vol. 45, no. 4, pp. 867–876, Apr 1998
[32] B. Winstead, U. Ravaioli: A quantum correction based on schroedinger equation applied to monte carlo device simulation, IEEE Transactions on Electron Devices, vol. 50, no. 2,, 2003
[33] J. Y. Tang, K. Hess: Impact ionization in of electrons in silicon (steady state), Journal of Applied Physics, vol. 54, no. 9, pp. 5139–5144, September 1983
[34] G. Gilat, Z. Kam: High-resolution method for calculating spectra of solids, Phys. Rev. Lett., vol. 22, no. 4, pp. 715–717, Apr 1969
[35] M. V. Fischetti, P. D. Yoder, M. M. Khatami, G. Gaddemane, M. L. Van de Put: Hot electrons in si lose energy mostly to optical phonons: Truth or myth, Applied Physics Letters, vol.114, no. 22, pp. 222104, 2019

BIOGRAPHY

Zlatan Akšamija was born on 6 July, 1980 in Sarajevo. He received his Bachelor of Science in Computer Engineering (Summa Cum Laude) in 2003, and his M.S. and doctorate in Electrical Engineering in 2005 and 2009, respectively, all from the University of Illinois at Urbana-Champaign, USA. His doctoral dissertation on “Thermal effects in semiconductor materials and devices” was supported by a Department of Energy Computational Science Graduate Fellowship. From 2009 to 2013, Zlatan was a Computing Innovation Postdoctoral Fellow and an NSF CI TraCS Fellow in the ECE department at the University of Wisconsin-Madison. In 2013, he became an Assistant Professor in the Electrical and Computer Engineering Department at the University of Massachusetts-Amherst and founded the NanoEnergy & Thermophysics lab, where he studies thermoelectric energy conversion and heat transfer in 2-dimensional materials and nanostructures. He was promoted to Associate Professor with tenure in 2019.